IEEE Access
Multidisciplinary | Rapid Review | Open Access Journal

Received January 15, 2021, accepted January 26, 2021, date of publication February 8, 2021, date of current version February 17, 2021.

Digital Object Identifier 10.1109/ACCESS.2021.3057906

Make It Trackable: An Instant Magnetic Tracking System With Coil-Free Tiny Trackers

RYO SHIRAI, (Graduate Student Member, IEEE), YUICHI ITOH, (Member, IEEE), AND MASANORI HASHIMOTO, (Senior Member, IEEE)

Department of Information Systems Engineering, Osaka University, Suita 565-0871, Japan

Corresponding author: Ryo Shirai (shirai.ryo@ist.osaka-u.ac.jp)

This work was supported by the Japan Society for the Promotion of Science (JSPS) KAKENHI under Grant JP19J11322.

ABSTRACT Ambient intelligence aims to actualize the environment that sense and utilize information around us without making us perceive the underlying systems. This work extends this concept by allowing us to track the movement and orientation of people and objects instantly. The proposed system can sense and let us know, for example, who met or talked to each other frequently, to whom s/he is often facing in the meeting, what stuffs people often use, where the person left his/her belongings, etc. Such information will help the system to understand the behavior patterns of each person and consequently can support and improve the personal life of users and even their mutual relationship. This article proposes an instant indoor magnetic tracking system that enables us to track the movement and orientation of people and objects by only attaching tiny electronic trackers to them. The size of the prototyped tracker is only 25.4mm × 25.4mm × 10.0mm, and hence it can be readily attached to almost anything and immediately activated. Evaluation results show that the proposed system applies to both room-scale tracking and tabletop scale tracking with 6 DoF (Degrees of Freedom).

INDEX TERMS Motion tracking, 6 DoF-sensor, ambient intelligence, dc magnetic field, 6-axis sensor.

I. INTRODUCTION

Ambient intelligence is an environment that allows us to take advantage of information gathered by distributed devices without making us aware of them. Ambient intelligence technology is expected to significantly improve our quality of life (QoL) by utilizing ambient information that has never been used and fed back to us so far.

There are various types of information that surround us, and they can be ultimately divided into two types: information that we are usually aware of or not. For example, the information that should be aware of includes Todo list, medical checkup, parking location, meeting schedule, and we manage them each time. On the other hand, we do not usually perceive where and when we used daily necessities, how long to whom we talked, in what posture we spent a day, etc. However, once we lose our property, or when we want to select the meeting participants most effectively, the information mentioned above will be needed immediately.

The associate editor coordinating the review of this manuscript and approving it for publication was Renato Ferrero.

Information that we are not aware of is further devided into two types: superficial information and non-superficial information. Superficial information, which includes, for example, the location of daily necessities, can be sensed physically, and is already utilized in a lost and found system with smart tag and a motion estimation system, etc. In contrast to superficial information, non-superficial one, which includes persons' mental status and degree of fatigue, etc., is difficult to sense directly. Meanwhile, the effectiveness of non-superficial information is implied by several research. K. Shiomi *et al.* point out that the human fatigue can be estimated by analyzing the voice of persons, and the workspace safety shall be improved by applying this information [1]. K. Kiyokawa *et al.* try to improve the user's working efficiency by building a system that monitors the user's drowsiness and concentration [2]. As these examples show, non-superficial information is expected to expand the application area of ambient intelligence, and therefore our QoL shall be improved. Here, an important point is that some of non-superficial information described above is related to the motion information. Notably, D. R. Carney *et al.* conducted psychological experiments and report that the posture

and behavior of persons are highly related to their feeling and mental status [3]. K. Kiyokawa *et al.* propose a smart office chair that can improve the office worker's QoL by automatically adjusting the tilt angle of the chair based on the his/her mental and physiological status estimated from the body motion [2]. These works demonstrate that motion information can enable us to gather not only superficial information but also non-superficial one, both of which contribute to ambient intelligence significantly. Therefore, the system sensing the posture and behaviour can not only assist us from the view of conveniences but also improve our physical and mental health.

Motivated by these observations, this article aims to realize ambient intelligence by tracking both the postures and movements of people and objects for enabling the system to estimate our health, human relationships, etc., which have been challenging to sense directly. In particular, we actualize and demonstrate an environment in which the positions and behaviors can be acquired by simply attaching a small tracker to each object or person while keeping our current living environment unchanged. The following explains the necessities of motion tracking and small-volume implementation.

As mentioned above, the unconscious activities and our mental states are interdependent, and hence the position, posture, movement direction, and speed of objects and humans are to be captured accurately. Fortunately, motion tracking is required by many existing applications, and then it has been studied for decades, and many findings and methods are presented (e.g., [4]–[6]). However, advanced ambient intelligence brings severer requirements for motion tracking than conventional applications, which include higher-level system robustness and instantness. Namely, ambient intelligence is expected to provide services in our daily environment instantly, and then the motion tracking should be able to start without any calibration and must work correctly in various situations. On the other hand, conventional methods are designed for specific applications, and then robustness and instantness problems are remaining, which will be discussed in Section II-B and Section III-A.

Another critical requirement is the volume reduction of the tracker. The motion tracking sensor must be implemented as small as possible since pervasive sensing is required for pursuing a wider application domain and a better user experience. The sensor volume reduction, on the other hand, enforces the low energy operation because the capacity of the battery which can be implemented in a small volume is severely limited. Nevertheless, to make the tracker applicable for many situations, the wireless communication function and high precision sensor circuit are required since wired trackers or imprecise motion tracking may miss unconscious activities reflecting our mental status. Furthermore, as mentioned above, we should be able to instantly provide a motion tracking function anywhere whose coverage area is large enough for the application of interest. Therefore, we conclude that the motion tracker for ambient intelligence should satisfy the following features.

- Sufficient robustness for daily environment
- Small volume
- Low installation cost
- Low energy
- Sufficient accuracy
- Adequate update frequency

To actualize the motion tracking system that satisfies the features listed above, we propose a DC magnetic field-based 3D motion tracking system. The proposed system localizes the tracker position with a single reference node in its minimal configuration while other methods often require numerous number of reference node. Our method does not require any site survey. These specifications greatly contribute to the low installation cost compared to other tracking methods. The coverage area is dependent on the size and the power given to the reference node only, and thus the scalability is ensured. The required update rate often depends on the system size since the tabletop system usually needs to sense fast and subtle movement caused by human hand compared to the body movement in the room-scale system. Therefore, we evaluate potentially available update rate in the tabletop scale. We achieved the update rate of 15.16 Hz by deriving and utilizing an approximate polynomial expression of the DC magnetic field instead of numerically calculating equations from the Biot-Savart law. Generally, magnetic tracking has to solve 3D field equations, which requires heavy computation. On the other hand, by deriving the approximation polynomial function, the proposed method allow us to find solution with O(1) calculation time, and then the calculation can be executed even with a laptop PC which has low computation power. The proposed method achieved the localization error with the maximum error of 9.69 mm in the tabletop environment. Also, the practicability of room-scale tracking is experimentally confirmed. Furthermore, we demonstrate that the localization performance sustains even in the background that contains a metallic obstacle since the proposed method is not affected by non-ferrous metallic materials.

II. RELATED WORK

This article is strongly motivated by the ambient intelligence technology, which utilizes the position and movement information of people and objects. Therefore, Section II-A will introduce several pieces of related research to explain the benefits potentially brought by ambient intelligence. Then, Section II-B will review currently available localization and motion tracking technologies.

A. AMBIENT INTELLIGENCE WITH TRACKING TECHNOLOGY

Internet of Things (IoT), which senses the information of all objects surrounding us and connecting the acquired information through the internet [7], [8], can be regarded as an infrastructure that supports ambient intelligence. A lot of IoT research has been conducted focusing on how to gather information and which information should be acquired from

environments [9]. On the other hand, applying IoT technologies to ambient intelligence, the concept of location-based service (LBS) gains its importance [10], [11] since the value of information elevates significantly when it is associated with the location information [12]. C. Perera *et al.* point out the importance of position estimation of an object because expected human-computer interaction greatly depends on its location and surrounding environment [11]. LBS plays an important role even when fusing the IoT and other new technologies. B. K. Kim *et al.* report that the estimation of object position facilitates the introduction of robot technology into our living environment [13]. Thus, detecting the position of an object is expected to promote various location-based services in our living environment and enhance our QoL.

Meanwhile, ambient intelligence utilizes not only ''things'' targeted by the IoT, but also information such as human positions and behavior. People output information during the conversation, working, and even when sleeping. Information emitted by a person includes not only verbal one but also non-verbal one such as body movement, the direction in which the person is facing, and the number of nodding actions during meetings, etc. Many researchers in both psychology and engineering fields have worked aiming at making conversations and meetings more effective and improving work environments with the assistance of information unconsciously emitted by people (e.g. [14], [15] [16], [17] [18]).

Especially, utilizing the position and behavior of a person as non-verbal information has been actively studied. T. Kim *et al.* try to improve the interaction within a group by utilizing the information of, for example, the people's movements during a meeting and the distance and positional relationship between participants [19]. K. Fujita *et al.* sense the hand and head movements and the number of utterances for estimating the participants' activities in a standing party [20], [21]. These studies report that the participants retain their activity at a high level when the estimated activity is fed back to them through a display installed on the wall and floor.

Collecting information via wearable sensors is also actively studied, aiming to realize ambient intelligence. K. Ara *et al.* collect behaviors and interactions of people in an organization with wearable sensors to realize and utilize the concept of ''business microscope [15].'' K. Ara *et al.* aim to enable organizations and people to work more efficiently in the future by understanding human behavior and make use of knowledge and information.

All the researches mentioned above attempt to create a society that utilizes ambient intelligence by sensing the positions and movements of objects and people in our living environment. These studies illustrate the effectiveness from different aspects of ambient intelligence, and therefore taking advantage of all aspects of ambient intelligence should improve our QoL significantly. On the other hand, each system listed above requires the installation of dedicated equipment and the environment for a specific purpose. Generally, this equipment and environment cannot be diverted to other systems. Therefore, the currently available researches cost significantly to introduce the equipment and environment for ambient intelligence.

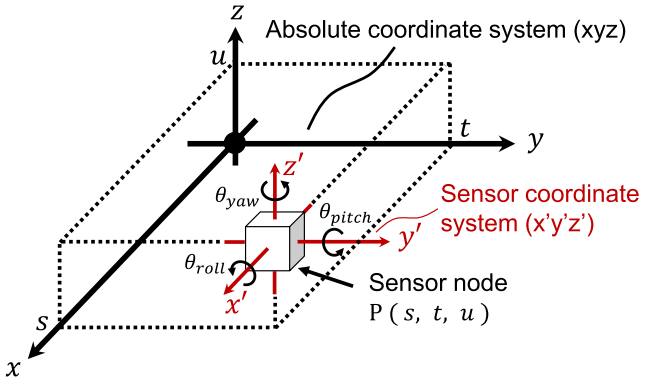

FIGURE 1. Motion tracking requires both position and posture estimation with 6-DoF.

For addressing this issue, our objective is set to developing a small volume motion tracker that can start to trace the movements of objects and people immediately after the attachment. Another issue is that currently available tracking technology may disturb our natural activity because of the existence of the relatively large equipment and systems. H. Müller *et al.* report that we have to prevent the user from being distracted when acquiring information and presenting information to the user; otherwise, the obtained information could be highly biased [22]. Thus, we conclude that the realization of an instant tracking system is the most vital part of actualizing the ambient intelligence-based society. The following section will review the currently available positions and motion tracking methods and examine whether they fit our objective.

B. TRACKING AND POSITIONING TECHNOLOGIES

Fig. 1 defines six variables $s, t, u, \phi_{roll}, \phi_{pitch}$, and ϕ_{yaw} that determine the posture and position of an object. Fig. 1 indicates that both of posture and position information have 3-DoF (Degrees of Freedom). Therefore, the motion tracking system that requires both posture and position estimation has to perform the 6-DoF estimation. For this reason, we review not only the existing motion tracking technologies but also the researches on localization and posture estimation. Fortunately, the posture estimation has a well-known method that can accurately estimate the posture of the sensor node based on the gravitational acceleration and geomagnetism [23], which will be explained in Section III-A. Therefore, this section focuses on the existing works on motion tracking and localization.

The most common position estimation method is a global positioning system-based (GPS-based) method, and its accuracy improvement is actively studied [24]. However, the GPS signal severely attenuates indoors and cannot provide enough accuracy. Also, the localization error of the GPS-based method is in meter scale in many cases, and hence it is not capable of sensing subtle object movement. Meanwhile, indoor localization methods, which can achieve cm-scale or

even mm-scale error, can be applied to motion tracking. Such indoor localization can be applied to many applications such as table-top localization and indoor navigation, and therefore numerous methods have been reported and tested [25].

M. Andries *et al.* develop load-sensing-floor that accurately estimates the positions of people and objects for the realization of ambient intelligence, where the load-sensing-floor is implemented with a large number of tiles consisting of multiple strain gauges [26]. This work suffers from installation cost and the difficulty in positioning small and light objects, and therefore it can be adopted only for some specific applications.

Camera-based motion tracking is a popular approach, and many works have been presented (e.g., [27]). Existing camera-based motion tracking methods can be divided into two types: methods based on the differences between several successive frames, and methods based on the marker attached to the object. D. Murray *et al.* propose a motion tracking method based on the frame differences and achieved high accuracy by compensating the camera pose. On the other hand, the camera-based method inherently involves an occlusion problem [28]. K. Kjærside *et al.* propose a marker-based motion tracking system that installs multiple cameras to avoid the occlusion problem [5]. However, the coverage area of this system is limited to a small space such as a dressing room, and it cannot be applied to a large space. Furthermore, the camera-based method has a privacy issue preventing dairy usage.

To avoid the privacy problem, the information other than the image is highly desirable for the position and posture estimation. D. Laurijssen *et al.* propose an ultrasound-based motion tracking method [29]. While it avoids the privacy problem, the occlusion problem still exists since obstacles seriously attenuate the ultrasound signal.

A solution to the occlusion problem is to utilize a signal that penetrates obstacles. For example, position estimation methods based on Wifi signals are widely studied (e.g. [30], [31] [32]) and some of them are already used for indoor localization. These methods achieve sufficient estimation accuracy for room-scale applications such as indoor navigation. On the other hand, the Wifi-based methods cannot be used for motion tracking since they cannot achieve cm- to mm-scale localization error.

On the other hand, some researches on the magnetic field-based method report that cm-scale or below estimation error is achievable. The magnetic field-based motion/location tracking methods can be divided into two types: AC magnetic field-based methods and DC magnetic field-based methods. Both methods are studied over decades, and hence many findings are reported and accumulated [33].

Let us first review AC magnetic field-based methods. W. Kim *et al.* theoretically demonstrate that we can estimate the position and posture of the sensor node with the AC magnetic signal [34]. J. Huang *et al.* have proposed a method to detect subtle movements of the fingertip with high accuracy using a large number of reference nodes in the distance of dozens of cm [35]. On the other hand, the tracking technology required for ambient intelligence, which is the objective of this research, emphasizes the lower installation cost rather than the extremely high accuracy and speed. Therefore the method utilizing many reference nodes is not suitable, and we should explore tracking methods that use a single reference node. K.-Y. Chen *et al.* and E. Whitmire *et al.* implement motion tracking using a handy reference node achieving high degrees of freedom [36], [37]. Similarly, S. Song *et al.* proposes a 3D localization method using only one reference node [38].

However, the AC magnetic field-based methods share the problem that the AC magnetic signal is significantly affected by not only ferrous materials but also non-ferrous metallic materials [39], although those materials are included in many of our everyday objects. Eq. (1) is the Maxwell-Faraday equation.

$$\mathrm{rot}\, E + \frac{\partial B}{\partial t} = 0, \tag{1}$$

where E and B are electric and magnetic fields, respectively. Eq. (1) indicates that when a conductive material is placed in an AC magnetic field, an eddy current flows inside the conductor. The eddy current generates a new AC magnetic field that interferes with the original AC magnetic field generated by the reference node. F. S. Parizi *et al.* and E. Whitmire et al, both of which propose AC magnetic field-based motion tracking methods, evaluate the impact of this weakness [40], [41]. The experiments performed by F. S. Parizi *et al.* and E. Whitmire et al revealed that non-ferrous metallic objects used in daily life, e.g., smartphones and personal computers, need to be placed at least 10 cm to 20 cm away from the system. Thus, the AC magnetic field-based approaches work correctly only in a specific environment where the metallic object is not positioned nearby. Our objective system should allow us to attach trackers to everything around us, including metallic objects mentioned above, and hence the AC magnetic field-based methods cannot be used.

In addition to this, the AC magnetic field-based systems suffer from the sensor volume problem, which is inevitable as long as the system utilizes the AC signal. The sensor node for the AC magnetic field has to be equipped with a coil. The tracking accuracy and precision strongly depend on the volume of the coil, and hence the sensor node has a larger size bound.

DC magnetic field-based motion tracking is drawing attention since it mitigates the robustness and sensor volume problems involved in the AC magnetic field-based methods. DC magnetic field can penetrate non-ferrous metallic material, unlike the AC magnetic field. Hence, DC magnetic field-based methods are inherently more robust than AC magnetic field-based methods. Also, the intensity of DC magnetic field utilized for the localization is a few mT or less and it does not affect the human body or medical devices such as pacemakers, and therefore, DC magnetic field based methods are much safer than AC magnetic based methods.

J. Blankenbach *et al.* propose DC magnetic field-based room-scale localization methods [42], [43]. P. H. Chen *et al.* propose a method that can extend the coverage area by placing new self-localizable reference nodes for tabletop applications [44]. All of these methods need multiple reference nodes for the localization. On the other hand, the multiple reference nodes-based methods are not suitable for our objective in terms of the installation cost. Therefore the method which can localize sensor nodes with a single anchor node is eagerly demanded.

S. H. Yoon *et al.* propose a finger-motion tracking method with the magnet installed on a daily object [45]. This method utilizes a permanent magnet as an excitation source, and the generated magnetic field is sensed by not coils but magnetometers. Thanks to the MEMS technology, the volume of these magnetometers is tiny, and then we can embed them into anything. On the other hand, these systems track only a single object since they use a permanent magnet and consequently cannot identify two or more objects. A similar permanent magnet-based method is proposed by Hu *et al.* [46]. However, this method estimates the position and orientation of the magnet with a large number of magnetometers, and hence the installation cost is high.

As a DC magnetic field-based method with the low installation cost, Reference [47] proposes a 3D localization method with a single reference node. Reference [47] achieves mm-scale localization accuracy and low system complexity, and it also reports the accuracy of the system does not degrade even in the environment where a non-ferrous metallic plate is installed. Hence, the method proposed in [47] is suitable for our system. On the other hand, this system is limited to 4 DoF, which means it can estimate the 3D position, but the posture information is missing. Therefore, we compensate for the posture information using the gravitational acceleration and geomagnetism, which we will explain in Section III-A. Here, posture information can also be compensated by a gyroscope [48], but the power consumption of gyroscopes is much larger compared to other sensors such as magnetometer and accelerometer, and hence we avoid using a gyroscope for our energy-limited tiny tracker.

As for the coverage area, the DC magnetic field-based system covers a narrower area than the AC magnetic field-based system. This problem on the coverage area comes from the signal propagation characteristic and the signal to noise ratio (SNR) [33]. While the signal voltage in the AC magnetic field-based system can be boosted by utilizing a higher frequency signal, DC magnetic field-based signal cannot be amplified without the active amplifier, which degrades SNR substantially. To overcome this coverage area problem, DC magnetic field-based methods have to give larger power to the reference coil compared to the AC magnetic field-based methods. Therefore the power consumption of the DC magnetic field-based method tends to be larger than that of the AC magnetic field-based method. For this reason, the DC magnetic field-based method is not suitable for the environment where a power outlet is not available. On the other hand, the objective of this work is to provide the indoor meter-scale tracking infrastructure, and the reference coil can be supposed to be powered from the power outlet. Therefore, this relatively larger energy consumption is not a crucial issue.

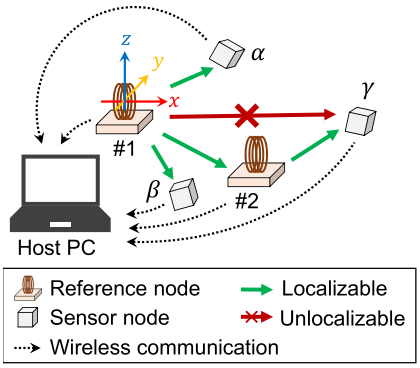

FIGURE 2. Overview of the proposed motion tracking method.

III. PROPOSED MOTION TRACKING METHOD

This section proposes a DC magnetic field-based motion tracking method with a single reference coil. As we explained in Section II, the motion tracking with the localization method proposed by [47] is promising in terms of robustness, instantness, and accuracy. However, this localization method is limited to 4-DoF estimation, and the other 2-DoF is missing. Therefore, this section explains a method that supplements 2-DoF with an accelerometer. Section III-A describes the outline of the proposed 6-DoF motion tracking method. Then, Sections III-C and III-D explain the details of the posture and position estimation methods, respectively.

A. OVERVIEW

Fig. 2 shows an overview of our motion tracking system. The host PC performs wireless communication with the sensor and reference nodes and estimates the posture and position of those with the gravitational acceleration and geomagnetism sensed by those nodes, where one sensor node corresponds to one tracker. In Fig. 2, reference node #1 provides an absolute coordinate system, which is depicted as *xyz*-coordinate system, and all the reference and sensor nodes should be localized in this absolute coordinate system. Each sensor and reference node senses the DC magnetic field generated by the reference nodes and sends the measurement results to the host PC via wireless communication. Then, the host PC calculates and estimates the positions of all the sensor and reference nodes from the obtained information.

The reference node has a constant current circuit and a reference coil in addition to the circuit installed in the sensor node. The reason why the reference node includes the sensor circuit is to ensure the system scalability. Let us explain with an example. In Fig. 2, sensor node γ and reference node #1 are too distant, and reference node #1 cannot localize sensor γ because of the attenuated magnetic field. Reference node #2 can localize sensor node γ on behalf of reference

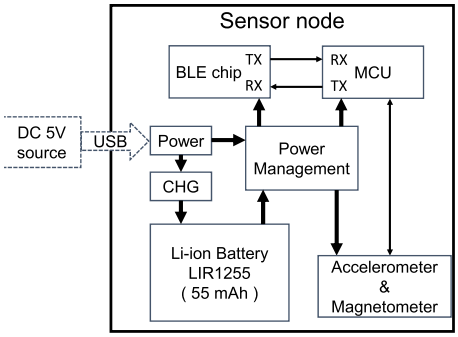

FIGURE 3. Structure of the sensor node.

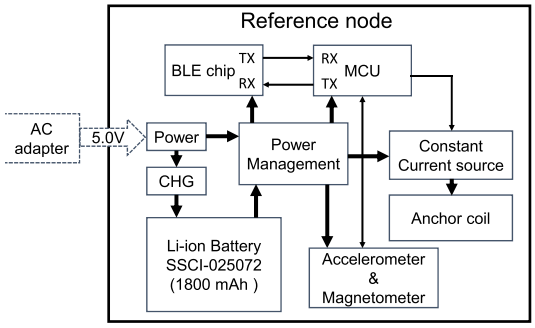

FIGURE 4. Structure of the reference node.

node #1. However, to localize sensor node γ according to the *xyz*-coordinate system, reference node #2 must know its own position and posture in the *xyz*-coordinate system. Therefore, reference node #2 localizes itself by sensing the DC magnetic field generated by reference node #1 with the sensor circuit mounted on itself. In this way, our method can extend the coverage area by simply adding the reference nodes, and hence the scalability is ensured. Here, Reference [47] has already reported experimental results showing that the coverage area expansion with multiple reference nodes is feasible. This article focuses on examining the feasibility of tracking with the tiny trackers, which can be attached to anything, for ambient intelligence. Therefore, the following section will discuss only the tracking ability and the performance with a single reference node.

Figs. 3 and 4 show the configurations of the reference and sensor nodes implemented in this work, respectively. The external 5V voltage sources shown in Figs. 3 and 4 are required only for charging the internal battery, and hence all the nodes can work wirelessly during the motion tracking. The sensor node consists of a power management circuit, an MCU (Micro Controller Unit), a 6-axis sensor (magnetometer and accelerometer), and a BLE (Bluetooth Low Energy) chip for wireless communication. As a 6-axis sensor, we adopt LSM9DS1 that includes not only an accelerometer and a magnetometer but also a gyroscope. Besides, the power consumption of the gyroscope is significantly larger than those of the other two sensors, and then we disable the gyroscope.

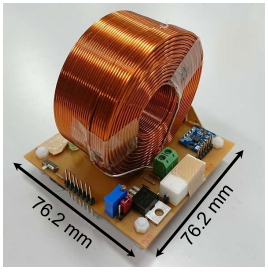

FIGURE 5. Prototyped reference node.

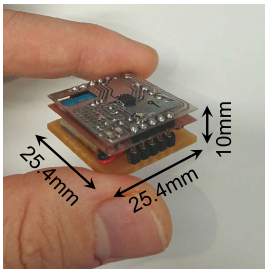

FIGURE 6. Prototyped thin sensor node used as a tracker.

The proposed method can provide a tracking service simply by installing a single reference node. The coverage area of a single reference node is determined by the amount of the power given to the reference coil and the coil size. Fig. 5 exemplifies the reference node for tabletop applications, and it supports a tracking service within a range of several dozens of centimeters. The volume of this reference node for tabletop applications is 76.2mm $\times$ 76.2mm $\times$ 76.2mm. Please note that we also implemented a large reference node for the room-scale tracking and conducted the experiment with it, which will be explained later in Section V.

This article aims to realize a small tracker that can be attached to everything around us. Therefore, the sensor node used as a tracker should be implemented not only in a small volume but also with thin thickness so that the attachment flexibility is much improved. Fig. 6 shows the appearance of the prototyped sensor node to be used as a tracker. This thin sensor node is implemented in a volume of 25.4mm $\times$ 25.4mm $\times$ 10mm. Users can instantly and immediately make any object or person trackable by attaching the tracker with double-sided tape.

The sensor node, of course, can be in any shape as long as it includes the circuits described above. Thus, we prototyped another type of cube-shaped sensor node shown in Fig. 7, which could be suitable for other applications (e.g., 3D modeling, game control). The function of the cube-shaped sensor node in Fig. 7 is identical to the thin sensor node in Fig. 6. Fig. 8 shows the disassembled cube-shaped sensor node. We can see that the volume of the 6-axis sensor mounted on the sensor board is tiny as it is 3mm $\times$ 3mm $\times$ 1mm. Therefore, we can implement the circuit for motion tracking even in a volume of mm^3 class by putting more effort into custom chip fabrication.

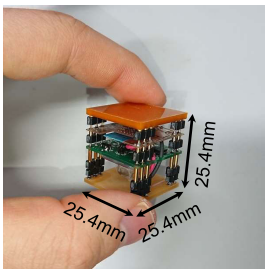

FIGURE 7. Prototyped cubic sensor node.

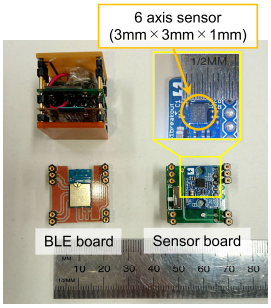

FIGURE 8. Disassembled cubic sensor node.

B. MOTION TRACKING PROCEDURE

This section explains the procedure of posture and position estimation performed in the system. The posture estimation uses gravitational acceleration and geomagnetism, which will be detailed in Section. III-C. Therefore, the system needs to order all the reference nodes to disable the reference coil. The system then commands all the reference and sensor nodes to measure geomagnetism and gravitational acceleration.

After all the reference and sensor nodes have completed the measurement, the system chooses one reference node and commands it to enable the reference coil in it. Then, all the sensor nodes and reference nodes except the selected reference node measure the DC magnetic field generated by the selected reference node. When all the nodes have completed the measurement of the artificially generated magnetic field, the system orders the same reference node to disable the coil and orders another reference node to enable the reference coil. Please note that no more than one reference node in the system enables the coil at the same time since all the reference nodes follow the single time division scheme controlled by the system.

After all the reference nodes have completed the coil activation and deactivation, the system now has the information on the gravitational acceleration, geomagnetism, and the magnetic field vector generated by the reference nodes at each sensor location. The system estimates the posture and position of all the reference and sensor nodes based on this information, which will be explained in the successive subsections.

C. POSTURE ESTIMATION

The position estimation method proposed by [47] supports posture estimation in addition to 3-DoF localization. However, this posture estimation is limited to 1-DoF. Therefore, 2-DoF is missing and must be compensated. In our method, the host PC estimates the posture of the sensor node with the 6-axis sensor. The sensor position and posture are represented by six variables $s, t, u, \phi_{roll}, \phi_{pitch}, \phi_{yaw}$, as we discussed with Fig. 1 in Section II. The posture estimation step estimates three variables $\phi_{roll}, \phi_{pitch}, \phi_{yaw}$ out of the six variables. These three angles denote Euler angles, and the posture of the sensor node is represented by the rotational matrix, which will be discussed later in this section.

Two important signals in the posture estimation step, which are gravitational acceleration and geomagnetism, are measured by a magnetometer and accelerometer, respectively. Here, as mentioned in Section III-A, all the posture and position estimation results should be based on the absolute xyz-coordinate system defined by reference node #1. On the other hand, the accelerometer and magnetometer installed in the sensor node output the information according to the $x'y'z'$-coordinate system, which is the original coordinate system of the sensor node. When there is no artificial magnetic field, which is caused by magnetic materials or coils, in the environment, the geomagnetic vector and the gravitational acceleration vector must be identical at an arbitrary point. Therefore, the posture difference between the reference and sensor nodes can be estimated by comparing the output differences of the magnetometer and accelerometer between the reference and sensor nodes [23]. Here, we define four variables as follows:

$$A_R = \begin{bmatrix} a_{Rx} \\ a_{Ry} \\ a_{Rz} \end{bmatrix}, \quad B_{Rd} = \begin{bmatrix} a_{Rxd} \\ a_{Ryd} \\ a_{Rzd} \end{bmatrix},$$
$$A_S = \begin{bmatrix} b_{Sx'} \\ b_{Sy'} \\ b_{Sz'} \end{bmatrix}, \quad B_{Sd} = \begin{bmatrix} b_{Sx'd} \\ b_{Sy'd} \\ b_{Sz'd} \end{bmatrix}, \tag{2}$$

where A_R and B_{Rd} are the accelerometer and magnetometer outputs of the reference node, respectively, and A_S and B_{Sd} are the outputs of the sensor node. These variables satisfy Eq. (3) below.

$$\begin{aligned} A_R &= R_z(\phi_{yaw})\, R_y(\phi_{pitch})\, R_x(\phi_{roll})\, A_S. \\ B_{Rd} &= R_z(\phi_{yaw})\, R_y(\phi_{pitch})\, R_x(\phi_{roll})\, B_{Sd}. \end{aligned} \tag{3}$$

Matrices $R_x(\phi)$, $R_y(\phi)$ and $R_z(\phi)$ in Eq. (3) are the rotation matrices around x-axis, y-axis, and z-axis, respectively, and they are defined as Eq (4).

$$R_x(\phi) = \begin{bmatrix} 1 & 0 & 0 \\ 0 & \cos\phi & -\sin\phi \\ 0 & \sin\phi & \cos\phi \end{bmatrix}.$$
$$R_y(\phi) = \begin{bmatrix} \cos\phi & 0 & \sin\phi \\ 0 & 1 & 0 \\ -\sin\phi & 0 & \cos\phi \end{bmatrix}.$$

$$R_z(\phi) = \begin{bmatrix} \cos\phi & -\sin\phi & 0 \\ \sin\phi & \cos\phi & 0 \\ 0 & 0 & 1 \end{bmatrix}. \quad (4)$$

To simplify the discussion, we assume $a_{Rx} = a_{Ry} = 0$, which means the gravitational acceleration vector is parallel to the z-axis and is a realistic assumption for most systems. In this case, the sensor posture $\phi_{roll}, \phi_{pitch}, \phi_{yaw}$ can be obtained as Eq. (5). Here, it should be noted that even if this assumption does not hold, that is, if the reference node is installed in an inclined plane, the tilt angle of the z-axis can be calculated with the first two equations in Eq. (5) by using A_R instead of A_S. Thus, the posture difference between the reference node and the sensor node can be obtained.

$$\begin{aligned} \phi_{roll} &= \text{atan2}\left(a_{Sy'}, a_{Sz'}\right). \\ \phi_{pitch} &= \text{atan2}\left(-a_{Sx'}, \sqrt{a_{Sy'}^2 + a_{Sz'}^2}\right). \\ \phi_{yaw} &= \text{atan2}\left(-\cos\phi_{roll} b_{Sy'd} + \sin\phi_{roll} b_{Sz'd}\right. \\ &\quad \cos\phi_{pitch} b_{Sx'd} + \sin\phi_{pitch}\sin\phi_{roll} b_{Sy'd} \\ &\quad \left. + \sin\phi_{pitch}\cos\phi_{roll} b_{Sz'd}\right) \\ &\quad - \text{atan2}\left(-b_{Ryd}, b_{Rxd}\right). \end{aligned} \quad (5)$$

Here, atan2(y, x) included in Eq. (5) is a function defined by Eq. (6), which extends the range of the arctangent function from $-\pi/2 < \phi < \pi/2$ to $-\pi \leq \phi \leq \pi$.

$$\text{atan2}(y, x) = \begin{cases} \tan^{-1}(y/x) & \text{if } x > 0, \\ \tan^{-1}(y/x) + \pi & \text{if } x < 0 \text{ and } y \geq 0, \\ \tan^{-1}(y/x) - \pi & \text{if } x < 0 \text{ and } y < 0, \\ \pi/2 & \text{if } x = 0 \text{ and } y > 0, \\ -\pi/2 & \text{if } x = 0 \text{ and } y < 0, \\ \text{undefined} & \text{if } x = 0 \text{ and } y = 0. \end{cases} \quad (6)$$

We derived Euler angles to represent the posture of the sensor node. Here, Euler angles have a disadvantage that a gimbal lock problem could occur and 1-DoF out of 3-DoF is missed if $\phi_{pitch} = \pm\pi/2$. Under the situation of the gimbal lock, the number of the combinations of $(\phi_{roll}, \phi_{pitch}, \phi_{yaw})$ representing the same posture is infinite. However, substituting any set of these values into Eq. (7), which will be explained in successive sections, gives the same result, and therefore 3-DoF is always obtainable. Also, it should be noted that we utilize the posture representation with Euler angles only for the position estimation procedure, which will be explained in the following section, and assume the application based on the proposed method does not necessarily utilize the derived Euler angles just as they are. If the application cannot tolerate the singularity explained above, we can transform the derived Euler angles into other variables (e.g. quartanion) which do not have the singularity.

This section explained the posture estimation based on the outputs from the accelerometer and the magnetometer. On the other hand, we need to pay attention to the fact that the output of the magnetometer usually contains some offset error, and it needs to be compensated beforehand. Generally, each sensor node needs its separate compensation, and hence the sensor installation cost can be relatively high. However, in this research, we assume that a large number of sensors are scattered in the environment. Hence, the newly installed sensor node can compensate its offset error using the data shared from previously installed adjacent sensor nodes. For this reason, the offset compensation will not be a big issue to adopt the proposed method for ambient intelligence.

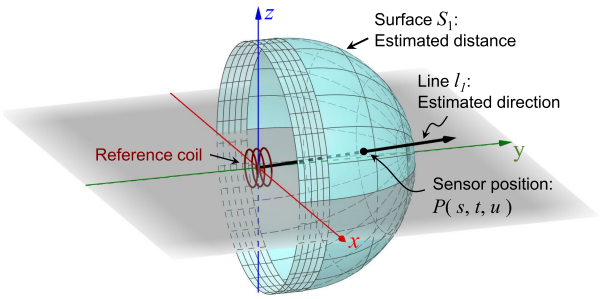

FIGURE 9. Overview of the localization method.

D. POSITION ESTIMATION

The sensor position estimation in this work uses the DC magnetic field-based localization method proposed by [47]. Let us briefly review this method. Fig. 9 shows an overview of the localization method with a single reference coil. The localization can be divided into two steps: distance estimation and direction estimation. The first distance estimation step estimates the distance between the reference coil and the sensor node using only the magnitude of the magnetic field measured by the sensor node. Then, it derives the equation of surface S_1 in Fig. 9. The subsequent direction estimation step estimates the equation of straight line l_1 representing the direction of the sensor node from the reference coil. This l_1 estimation is based on the direction information of the magnetic field measured by the sensor node. The intersection of surface S_1 and line l_1 is uniquely determined, and then the position of the sensor is identified. Following Sections III-D1 and III-D2 describe the details of the distance and direction estimation, respectively.

1) DISTANCE ESTIMATION STEP

This step derives contour surface S_1 corresponding to the distance from the reference coil to the sensor $P(s, t, u)$. The localization requires the posture estimation results, which are explained with $\phi_{roll}, \phi_{pitch}, \phi_{yaw}$, and the geomagnetism vector B_{Sd} measured in the posture estimation phase. Let $B_{Pe} = [b_{Px'e}, b_{Py'e}, b_{Pz'e}]$ denote the output of the sensor node when the system is injecting current to the reference coil. Here, B_{Pe} includes not only the magnetic field $B_P = [b_{Px'}, b_{Py'}, b_{Pz'}]$ generated by the reference coil but also the geomagnetism B_{Sd} which has to be removed for localization. Then, to obtain B_P, we calculate $B_P = B_{Pe} - B_{Sd}$ and eliminate the effect of geomagnetism. In addition to this, since B_P is expressed according to the $x'y'z'$-coordinate system,

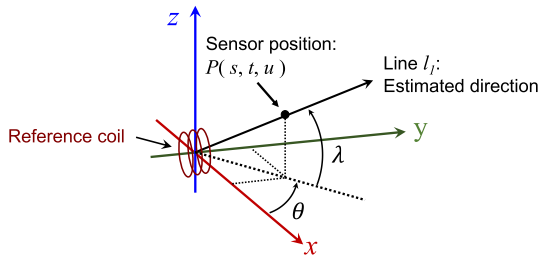

FIGURE 10. Line l_1 and definition of λ and θ.

we perform coordinate transformation:

$$B_{Pt} = [b_{Pxt}, b_{Pyt}, b_{Pzt}] = R_z(\phi_{yaw})\, R_y(\phi_{pitch})\, R_x(\phi_{roll}) B_P. \quad (7)$$

According to [47], the equation of the surface S_1 is expressed as follows:

$$S_1 : \begin{cases} x^2 + \left(y - \frac{1}{4} r_0\right)^2 + z^2 = r_0^2 & \text{if } |y| > \frac{1}{4} r_0, \\ x^2 + z^2 = r_0^2 & \text{otherwise,} \end{cases} \quad (8)$$

where r_0 in Eq. (8) is defined by Eq. (9).

$$r_0 = \left(\frac{|B_{Pt}|}{\alpha}\right)^{-\frac{1}{\beta}}, \quad (9)$$

where α and β are approximation constants. When the coil specifications are given, α and β are easily obtained since the magnitude and direction of the DC magnetic field generated by a single reference coil at an arbitrary point can be calculated analytically [49]. With these approximations, the proposed method does not have to solve the 3D electromagnetic field equations, which require heavy computation to obtain the solutions, and hence the low computational cost is achieved.

2) DIRECTION ESTIMATION STEP

The objective of the direction estimation step is to derive the equation of line l_1. As shown in Fig. 10, line l_1 is determined by two angles: λ and θ. Here, λ and θ are calculated as follows:

$$\begin{aligned} \lambda &= \text{atan2}\,(b_{Pzt}, b_{Pxt}), \\ \theta &= a_\theta \xi^3 + b_\theta \xi^2 + c_\theta \xi + d_\theta, \end{aligned} \quad (10)$$

where $a_\theta, b_\theta, c_\theta$, and d_θ are approximation constants which are derived by the relationship between the reference-sensor direction and the direction of magnetic field. Reference [47] provides a method to obtain $a_\theta, b_\theta, c_\theta$, and d_θ. Note that $a_\theta, b_\theta, c_\theta$, and d_θ are values unique to the coil used for the reference node and needs to be obtained only when we adopt a new reference coil. Once we obtain the combination of $a_\theta, b_\theta, c_\theta$, and d_θ for a specific reference coil, we can obtain θ only by substituting ξ to Eq. (10). ξ is defined by Eq. (11).

$$\xi = \pi/2 - \text{atan2}(b_{Pyt}, b_{Pzt} \sin\lambda + b_{Pxt} \cos\lambda). \quad (11)$$

The intersection of surface S_1 and line l_1 represents the position of the sensor node $P(s, t, u)$ and is expressed as follows:

$$\begin{aligned} s &= t \cos\lambda. \\ t &= \frac{r_0}{4} \tan^2\left(\frac{\pi}{2} - \theta\right) \frac{1 + \sqrt{16 + \frac{15}{\tan^2\left(\frac{\pi}{2} - \theta\right)}}}{1 + \tan^2\left(\frac{\pi}{2} - \theta\right)}. \\ u &= t \sin\lambda. \end{aligned} \quad (12)$$

IV. HARDWARE EVALUATION

This section validates the proposed method and examines the performance of the proposed system. Here, tracking in a small area often requires higher accuracy and update rate, whereas tracking in a wider area may tolerate relatively larger error and the low update frequency. For example, in a table-top application, the system should provide tracking with a maximum error of several mm at an update rate of at least several Hz. On the other hand, when it comes to room-scale ambient intelligence, the system can tolerate a tracking error of several cm, and the update rate can be even reduced to around 1 Hz [50]. Therefore, the hardware evaluation in this section focuses on table-top tracking having the severer performance requirements. We utilize a coil whose diameter is ϕ68 mm × 30mm, and inductance is 10 mH as the reference coil for the tabletop-scale application, which is found in Fig. 5. The current injected to the reference coil is set to 1 A. As for room-scale tracking, Section V-C will show use cases in the range of several meters from the reference node.

Section IV-A evaluates the accuracy of the 3-DoF posture estimation of the sensor node. Section IV-B shows the localization accuracy of the proposed method. Then, SectionIV-C shows the performance of the motion tracking function, and Section IV-D evaluates the speed and update frequency of the proposed motion tracking system.

A. POSTURE ESTIMATION

1) SETUP

This section evaluates the posture estimation performance of the proposed system. As we discussed in Section II-B, the posture of the sensor node has 3-DoF expressed with three variables $\phi_{roll}, \phi_{pitch}, \phi_{yaw}$. This section discusses the 1-DoF estimation followed by the 3-DoF estimation.

To fix the sensor posture in specific inclination angles, we made a gimbal which can retain the sensor node. The gimbal is made of wood so that the magnetic field around the sensor node is not disturbed. The gimbal uses several screw holes to fix the sensor node to a specific angle, and hence the error of installation angles is mitigated and is less than 0.3 degrees.

Some tabletop-scale applications require the real-time update and consequently cannot average many samples. Therefore, the system should be evaluated not only with the accuracy but also with the precision, where please remind that accuracy means how close the average value is to the actual value, and precision represents the variance of the measurement data.

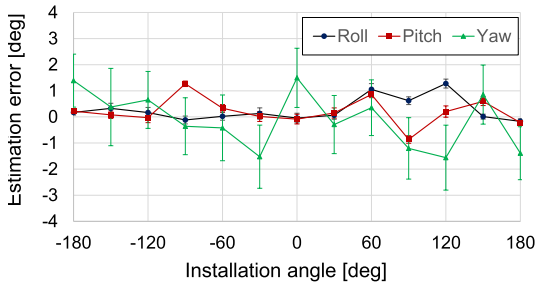

FIGURE 11. Angle estimation errors of 1-DoF posture estimation.

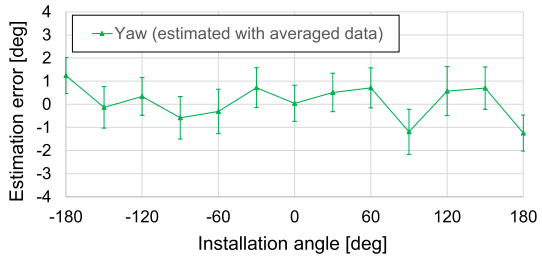

FIGURE 12. Result of yaw angle estimation based on the averaged sensor output.

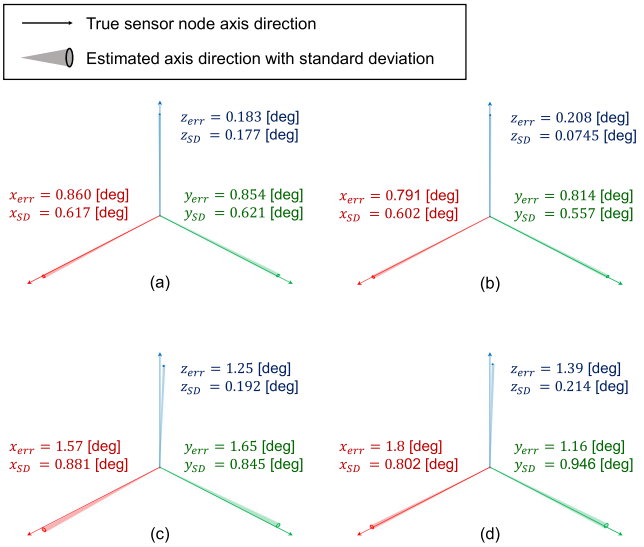

FIGURE 13. 3-DoF posture estimation result with various installation angles. (a):$(\phi_{roll}, \phi_{pitch}, \phi_{yaw}) = (0, 0, 0)$[deg], (b):$(\phi_{roll}, \phi_{pitch}, \phi_{yaw}) = (45, 0, 0)$[deg], (c):$(\phi_{roll}, \phi_{pitch}, \phi_{yaw}) = (45, 45, 0)$[deg], (d):$(\phi_{roll}, \phi_{pitch}, \phi_{yaw}) = (45, 45, 45)$[deg].

2) RESULTS

Fig. 11 shows the angle estimation results when two angles out of $\phi_{roll}, \phi_{pitch}, \phi_{yaw}$ are set to 0 degree and only one angle is changed from -180 to 180 degrees. To show the static performance of the 1-DoF estimation, we estimated each angle 10,000 times. Fig. 11 plots the averages and standard deviations of the estimation errors to examine the accuracy and precision at the same time. The average estimation error of each angle is less than ± 2 degrees, which means the posture estimation method based on the gravitational acceleration and geomagnetism can estimate 1-DoF angle with high accuracy. Focusing on ϕ_{roll} and ϕ_{pitch}, the standard deviations are less than 0.23 degrees, and the system can achieve precise estimation. As for ϕ_{yaw} estimation, on the other hand, the standard deviation is 1.48 degrees at maximum, and the precision is lower compared to ϕ_{roll} and ϕ_{pitch} estimation. This difference originates from the precision difference between the accelerometer and magnetometer. Variable ϕ_{yaw} is estimated from the magnetometer output with a large standard deviation, while the other two variables ϕ_{roll} and ϕ_{pitch} are estimated from the accelerometer output with a small standard deviation. Here, the magnetometer embedded in the 6-axis sensor of our system supports the data averaging [51] and can mitigate the output variation. Fig. 12 shows the ϕ_{yaw} estimation result with this averaging function. The averaging function reduces the standard deviation from 1.48 to 1.06 degrees and contributes to the higher precision. However, further averaging lowers the data rate and causes an insufficient update rate problem. Therefore, our system just utilizes the averaged sensor output and does not conduct further averaging. The precision problem regarding motion tracking performance will be discussed in Section IV-C.

Fig. 13 shows the 3-DoF posture estimation results, where all the variables $\phi_{roll}, \phi_{pitch}, \phi_{yaw}$ are changed simultaneously. We selected four combinations of $(\phi_{roll}, \phi_{pitch}, \phi_{yaw}) =$ (a): (0, 0, 0), (b): (45, 0, 0), (c): (45, 45, 0), and (d): (45, 45, 45) in consideration of symmetry. Each posture is estimated 10,000 times and the average and standard deviation of the estimation error are calculated. In Fig. 13, x_{err} denotes the average angle estimation error in the x-axis of the sensor node, x_{SD} is the standard deviation, and the same for the y-axis and z-axis. Fig. 13 shows that the system can estimate the sensor axis directions with the maximum estimation error of 1.65 degrees and the standard deviation is 0.946 degrees at maximum at any posture. In our daily environment, most applications tolerate the posture estimation error of 1.65 degrees, and then we conclude that the system can estimate the posture of the sensor with sufficient accuracy and precision. Meanwhile, the posture estimation error affects the localization performance. Therefore, we will discuss the impact of the posture error on the localization accuracy in Section V-A.

B. LOCALIZATION

1) SETUP

This section evaluates the localization performance of the proposed method. To show the localization performance in the table-top scale, we set the evaluation area to $0 \leq x \leq 300$ [mm], $0 \leq y \leq 300$ [mm], $0 \leq z \leq 200$ [mm]. We evaluated the localization 500 times for each sensor position to show the stabilized result. The localization requires the switching of reference nodes, and therefore, the localization experiment takes longer time compared to the posture estimation experiment. For this reason, the evaluation count is 500, whereas it was 10,000 for posture estimation in Fig. 11.

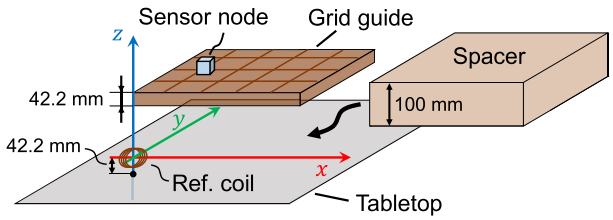

FIGURE 14. Installation of the sensor node.

The setup of the sensor node installment is shown in Fig. 14. As a guide for installing the sensor node, we made a wooden board with a grid mark whose interval was 50 mm. The grid is printed within the error of 0.01 mm, and hence the grid error is negligibly small for our localization experiment. On the other hand, we manually placed the sensor node using the grid mark. This manual placement error is included in the experimental results, but it could be at most 0.2mm. Here, the thickness of the grid guide is 42.2 mm within the error of 0.01 mm, where the thickness is equivalent to the distance between the tabletop and the center of the reference coil. The origin of the absolute coordinate system is set to the center of the reference coil. When we change the z-coordinate of the sensor node, we insert one or two wooden planks whose thickness is 100 mm as spacers just under the grid board described above. The thickness errors of these spacers were also less than 0.01 mm.

2) RESULT

Fig. 15 shows the localization results in the area of 300 mm × 300 mm × 200 mm. The black points are the actual positions, the red cross marks are the positions estimated as the averages of 500 estimates, and the black bars around the red cross mark denotes the error bars corresponding to one standard deviation. The reference coil is positioned at (0, 0, 0). Fig. 15 indicates that accuracy and precision are high near the reference coil. On the other hand, both the accuracy and precision deteriorate at the points apart from the reference coil. Nevertheless, as the static localization performance, the system achieves the maximum localization error of 9.69 mm in the range of 350 mm from the reference coil. Please note that the localizable area is four times larger than the result shown in Fig. 15 since the localizable area of our method is axially symmetric to the y-axis while Fig. 15 shows the result only in the region of $x \geq 0, z \geq 0$.

C. MOTION TRACKING

1) SETUP

This section evaluates the motion tracking performance of the proposed method in two situations: the environment without and with non-ferrous metallic material. Motion tracking requires dynamic position estimation, while ordinary localization requires static position estimation. In the motion tracking, the sensor position changes over time, and then we cannot average many samples. Therefore, it is more difficult than static localization. Accordingly, the system calculates

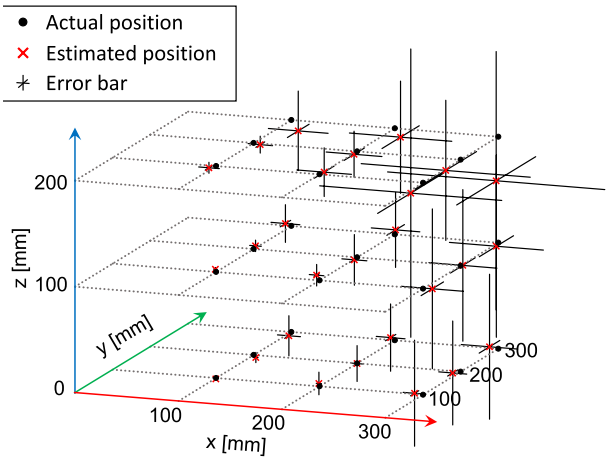

FIGURE 15. 3D localization result.

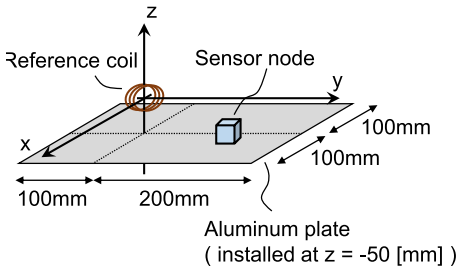

FIGURE 16. Motion tracking with aluminum plate.

and uses the average value of the latest 20 localization results, which means the data rate is unchanged while minimizing the effect of error fluctuation. We moved the sensor location with fingers at the speed of approximately 2.5 cm per second. For this reason, tracking results include the localization error originating from the speed fluctuation, i.e., acceleration. On the other hand, our objective is to track the sensor movement caused by humans as described in Section I. Therefore, we can say the presented results below shows the tracking performance in a practical situation.

One of the advantages of our system is the robustness to non-ferrous metallic materials, which are common in our daily environment, as we explained in Section II. To confirm this robustness, we also examine the motion tracking performance with the setup of Fig. 16, where a large aluminum plate whose thickness is 4 mm is installed at $z = -50$ [mm]. Please remind that the AC magnetic field-based methods are disturbed by the plate and they cannot localize or track the sensor position at all. In obtaining one trace both with and without aluminum plate, the system performs the posture and position estimation 300 times in total. The update frequency of the system is fixed to 6.25Hz to guarantee stable wireless communication.

2) RESULTS

Fig. 17 shows the tracking results without aluminum plate. Fig. 17 indicates that our motion tracking system can track the

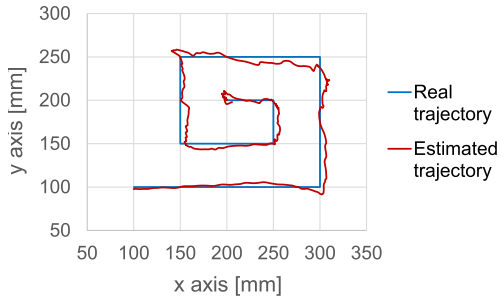

FIGURE 17. Motion tracking result.

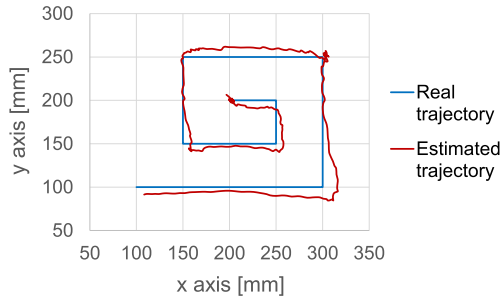

FIGURE 18. Motion tracking result with aluminum plate.

sensor position accurately, even with the single reference coil and small 6-axis sensor. The average motion tracking error in Fig. 17 is 4.26 mm, which indicates that the proposed method can provide sufficient accuracy for tabletop application.

Fig. 18 shows the motion tracking result with the aluminium plate. The average tracking error in Fig. 18 is 5.15 mm. In Fig. 18, we did not find a significant deterioration even when the aluminum plate was placed just below the tracing area, as we expected from [47]. Besides, the motion tracking of the proposed method is performed by conducting the localization repeatedly as described above. Therefore, the motion tracking characteristic is characterized by a set of positioning errors at individual points. Then, we make histograms of the tracking error in both situations to quantitatively evaluate the difference. Here, the number of the localizations performed in each experiment is 300, as we mentioned earlier. Fig. 19 shows the error distribution during the motion tracking in each situation. Fig. 19 indicates that most of the tracking errors are within 12.5mm in both the situations. When the aluminum plate is installed in the environment, several errors exceeding 12.5 mm occur, and hence the tracking result is slightly degraded. However, as we described above, the average tracking error deterioration is limited and less than 0.9mm.

Here, we moved the sensor node at an almost constant speed so that acceleration of the sensor node got close to zero. Our tracking method utilizes the gravitational acceleration and consequently the acceleration involved with the node movement disturbs the measurement of gravitational acceleration. In other word, our method cannot track the sensor node during acceleration, which is a limitation of the proposed method. On the other hand, this work aims to

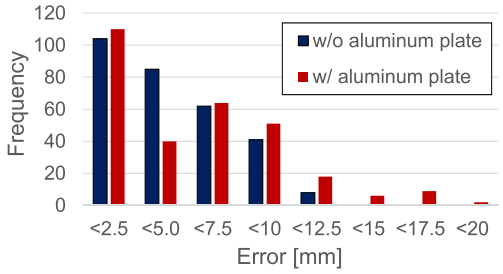

FIGURE 19. Distribution of tracking error at each point.

TABLE 1. Time profile of each function.

Function	Execution time [ms]
BLE communication	55.01
Overhead in host PC	6.20
Overhead in MCU	4.77
Total time	65.98 (15.16 Hz)

track movements of persons and objects moved by humans as described in Section I. Those movements do not always accelerate: they often stop or move at a constant speed. Also, the proposed system tracks the position of the sensor not only while the sensor is stopping, but also while sensor is moving at a constant speed. In this case, as long as we focus on the movement caused by humans, the position information while the sensor is accelerating shall be complemented from the position information before and after the acceleration. Therefore, the limitation described above is not a serious issue in the application field of interest. Note that if we have to track the objects which are constantly accelerating, we should compensate the tracking information with gyroscope or other sensors. In particular, the gyroscope has good response characteristics in the high frequency region compared to the accelerometer, and hence it can effectively compensate the impact of the acceleration.

D. UPDATE FREQUENCY

Table 1 shows three key factors that determine the posture and location update rate of the current prototype: BLE communication, the overhead in the host PC, and the overhead in the MCU. The time required to finish each cycle is 65.98 ms, and the achieved update rate is 15.16 Hz. In Table 1, BLE communication includes only the communication from the host PC to the sensor node because the communication from the sensor node to host PC, which takes a shorter time of 52.47 ms, is completed in parallel to the host PC to sensor communication. Apart from the wireless communication, the reference coil utilized in our method has a large inductance of 10 mH, and therefore it takes time to stabilize the current flowing through the coil. Fig. 20 shows the current change after the constant current source starts to inject the 1A current to the reference coil. The experiment is conducted in two environments, where one contains an aluminum plate, as shown in Fig. 16, and the other does not. Fig. 20 shows that the required time for the current stabilization is almost identical in both the environments, and the required time is

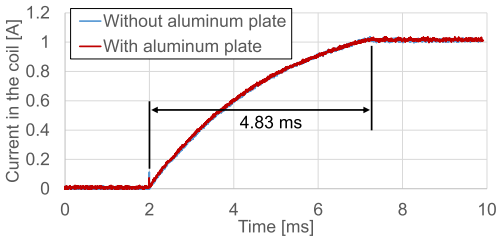

FIGURE 20. Stabilization of the current flowing through the reference coil.

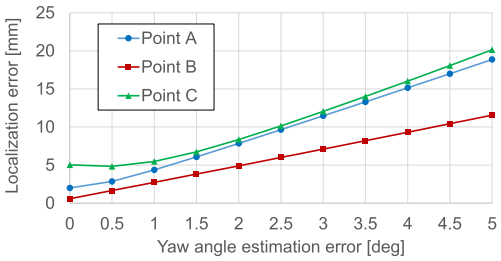

FIGURE 21. Localization error caused by the yaw estimation error.

4.83 ms. Both coil-enabling and coil-disabling take nearly the same time, and hence the coil related function takes $4.83 \times 2 = 9.66$ ms in total. Here, the time of 9.66 ms is much shorter than the time required for wireless communication. The measurement time of the sensor takes relatively long time compared to the coil switching, which will be further discussed in Section V-B, but not exceed 15 ms. For these reasons, the coil enabling/disabling and measurement are all done in parallel to the BLE communication. Hence, those do not affect the update rate in the current configuration. Thus, the current update rate is mostly determined not by the measurement or computation but by the BLE communication. Therefore, if the wireless communication speed is enhanced, the entire update rate is significantly improved. Section V-B will introduce the execution times of other functions and discuss the achievable update rate of our motion tracking system.

V. DISCUSSION

This section discusses further details about the characteristics of the proposed motion tracking system. Section V-A investigates the localization error originating from the posture estimation error. Section V-B discusses the potentially available tracking speed supposing that the performance of the wireless communication circuit is sufficiently enhanced. Section V-C introduces some motion tracking examples in non-laboratory daily environments.

A. LOCALIZATION ERROR INDUCED BY POSTURE ESTIMATION ERROR

As we explained in Section III, our motion tracking method consists of two steps: 3-DoF posture estimation followed by 3-DoF localization. The localization step requires the estimated posture for the coordinate transformation from the sensor coordinate system to the absolute coordinate system, as we explained in Section III-D. Therefore, the posture estimation error invades the localization error through the coordinate transformation. To investigate the influence of the posture estimation performance on the localization error, we conduct a simulation experiment. For evaluating the effect of the estimation error of a single variable on the localization error, we here assume that only ϕ_{yaw} contains the error and the other two variables, ϕ_{roll} and ϕ_{pitch}, are correctly estimated. Eqs. (7), (10), and (11) indicate that the yaw estimation error propagates to λ, ξ, and θ. ξ is utilized to derive θ, and consequently, the yaw estimation error causes estimation errors of λ and θ, where λ and θ determine the anchor to the sensor direction. To simplify the discussion and focus on the impact of the single variable, we assume $\lambda = 0$, which means all sensor nodes are located in the $xy-$plane. Let three sensor nodes be placed at points $A(100, 300, 0)$, $B(300, 100, 0)$, and $C(300, 300, 0)$, respectively. We also assume all of the sensor axis match the absolute coordinate system, which means $(\phi_{roll}, \phi_{pitch}, \phi_{yaw}) = (0, 0, 0)$, while the estimated ϕ_{yaw} contains error.

The simulation result in Fig. 21 shows that the yaw estimation error degrades the localization accuracy. The localization errors become larger linearly as the yaw estimation error increases. Fig. 21 also indicates that the error increasing rate at point C is more significant than those at points A and B. The distance between point C and the reference node is larger than those of points A and B, and hence subtle angle estimation error results in a significant localization error in the xyz space. Here, we limited the discussion to single variable θ and assumed $\lambda = 0$. If $\lambda \neq 0$, both λ and θ affect the localization error, which would result in a larger error. The discussion revealed that the effect of the yaw estimation error is considerable, even in $\lambda = 0$ situation. Therefore, to enhance the localization accuracy at the points apart from the reference node, we should improve the posture estimation accuracy first.

Besides, apart from the posture estimation error, in Fig. 21, we can see that the localization error cannot be zero even when the yaw estimation error is zero. This error originates from the approximation function explained in Section III-D and can be suppressed by introducing LUT (Look Up Table) or another more precise approximation function.

B. POTENTIALLY AVAILABLE TRACKING SPEED

The update rate of the proposed motion tracking method is determined mostly by the BLE communication in the current configuration, as we explained in Section IV-D. For future system enhancement, on the other hand, this section discusses the potentially available motion tracking speed supposing that the wireless communication speed is sufficiently enhanced.

There are two fundamental functions executed in the proposed system: enabling and disabling the reference coil, and the measurement. As we described in Section IV-D, the switching time of the reference coil cannot be shorter than

TABLE 2. Time profile of each function.

Function	Execution time [ms]
Measurement of magnetic field	12.9
Measurement of acceleration	1.05
Coil enabling/disabling	9.16
Overhead in host PC	6.20
Overhead in MCU	4.77
total	34.58 (28.92 Hz)

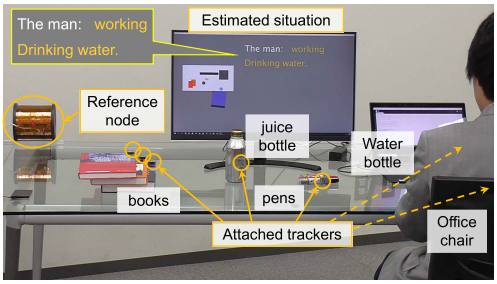

FIGURE 22. The system installed in an office environment with the proposed tracking technology provides a service based on ambient intelligence. The display indicates the estimated situation in addition to the locations of the objects with the trackers.

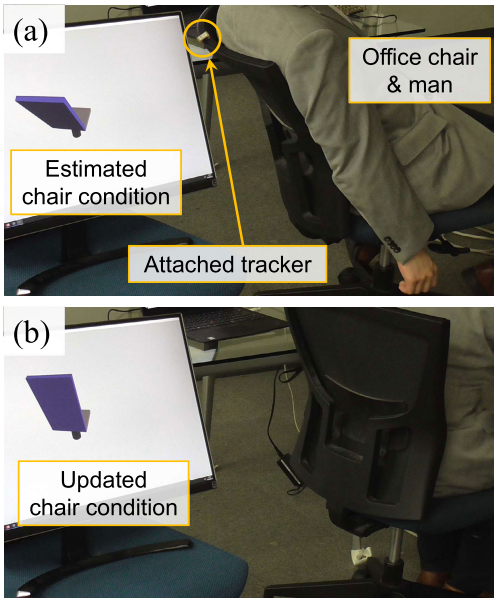

FIGURE 23. A tiny tracker attached to the backrest enables the system to estimate the office chair condition.

9.66 ms. Also, the sensor node requires the measurement time of accelerometer and magnetometer, and it includes overheads in the host PC and the MCU of the node. Table 2 listing those necessary times indicates that the system requires at least 34.58 ms for each localization, and hence the potentially available update rate is 28.92 Hz. Here, please note that the required time for the current stabilization depends on the maximum voltage applied to the coil. Therefore, the potentially available update rate can be higher than 28.92 Hz if we tune the hardware so that the constant current source can drive higher voltage.

C. EXAMPLE IN USE

Finally, this section sets up some potential use cases and conducts experiments to demonstrate the practicality and the robustness of our motion tracking system. The experiments in this section are recorded in a demonstration video. Please see the video as well.

The purpose of this article is, as we mentioned several times, to actualize ambient intelligence with an instant motion tracking system. Therefore, we implemented dozens of trackers and evaluated whether our tracking method can contribute to actualizing ambient intelligence based on LBS. In the proposed system, each tracker is identified by the ID number assigned for wireless communication, and therefore the system can track multiple sensors at the same time.

Fig. 22 shows the experimental environment and the system output via the LCD. Fig. 22 illustrates that the system estimates not only the position of the trackers but also the working status of the officer and his behavior. In this example, the system estimates the circumstance based on the object positions and the direction of the chair backrest. If the water bottle is moved to near the officer, the system considers that the officer is drinking water. As for the officer's working status, the system monitors the output of the tracker attached to the chair backrest and estimates the condition of the office chair, as shown in Fig. 23. By sensing the conditions of the office chair, the system can know, for example, whether the officer is working, relaxing, or absent. Thus, the experiment confirms the feasibility of the potential applications and shows that the proposed motion tracker can contribute to ambient intelligence. On the other hand, in this preliminary experiment, we simply made a look-up-table which associated several statuses with the posture and position of the sensor nodes beforehand. Further study on status estimation is necessary. Needless to say, machine learning techniques help improve the status estimation regarding robustness and accuracy and advance the services.

The trackers proposed in this article can be attached to not only objects but also men. When we attach the trackers to men, the system can estimate, for example, who met or talked to each other frequently, to whom s/he is often facing in the meeting, etc. For the demonstration, we attached the trackers to two men and conducted an experiment. Fig. 24 shows that the system estimates two men are talking to each other based on the positions and directions of them and the facing duration.

The example use cases introduced above require the meter-scale motion tracking, which is indispensable to actualize a room-scale ambient intelligence. The experiments here demonstrate that our proposed system with a larger reference coil is also applicable to meter-scale motion tracking. The experiments in in Section IV, on the other hand, have demonstrated that our system can also apply to the tabletop applications, which require a higher update rate and higher tracking accuracy. Also, our system can work in a harsh environment

TABLE 3. Comparison with related work.

	[35]	[40] [41]	[38]	[42] [43] [44]	[45]	This work
Mag. Signal type	AC	AC	AC	DC	DC(magnet)	DC
Single ref. node	No	Yes	Yes	No	Yes	Yes
Multiple sensors	Yes	Yes	Yes	Yes	No	Yes
Tracking distance	Dozens of cm	Several cm	Dozens of cm	Several meters	Several cm	Several meters
Tracking accuracy	1mm	Several mm	1.1 mm	Several cm	8.6 mm	5.15 mm
Non-ferrous metal	Intolerable	Intolerable	Intolerable	Tolerable	Tolerable	Tolerable
Scalable	No	Yes	Yes	Yes	No	Yes

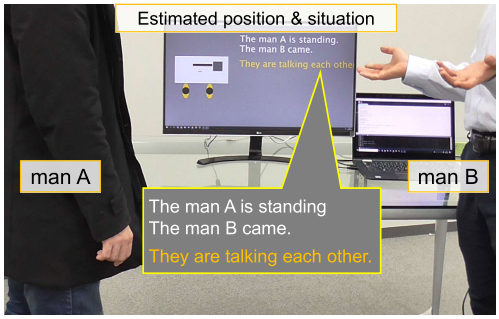

FIGURE 24. The proposed system successfully estimates the positions and directions of the men with the trackers and, as a result, recognizes the situation that they are talking each other.

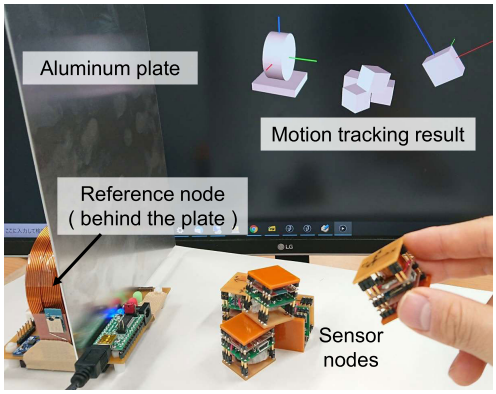

FIGURE 25. The proposed system can track the sensor nodes even when the reference node is occluded by a metallic plate.

that contains a metallic obstacle. Fig. 25 demonstrates that the system can track the sensor nodes even under the occlusion with the metallic plate. Thus, the robustness of our proposed system is experimentally confirmed.

D. COMPARISON WITH RELATED WORKS

Table 3 shows the comparison with related works on magnetic field based motion tracking or localization. Table 3 indicates that DC magnetic field based methods tolerate non-ferrous metallic obstacles while AC magnetic field based methods do not allow the metallic obstacle locating in the tracking area. Reference [45], which is even DC magnetic field based method, suffer from the scalability problem, while this work overcomes it with the feature of self-localizable single reference node. This work achieved the same level of tracking error as other related works, even though this work achieves relatively large tracking area, low installation cost with single reference node, and the practicability that the system is not disturbed by the daily non-ferrous metallic material. For these reasons, the proposed motion tracking method can be a solution for robust and instant motion tracking systems.

VI. CONCLUSION AND FUTURE WORK

This article proposed a DC magnetic field-based 6-DoF motion tracking method with a single reference node. The proposed method is suitable for motion tracking in the daily environment since it can provide not only instant but also robust motion tracking even in the environment containing daily obstacles, which possibly cause occlusion problems and contain metallic material. The proposed method does not require any complex hardware structure or intensive computation, and hence motion tracking is readily enabled. The sensor node, which is used as the tracker, is small and thin, and hence we can attach it to anything around us. This instantness of the proposed method highly contributes to building the infrastructure for ambient intelligence. Although the demonstrated use cases aim to show the feasibility of the instant tracking in the room-scale environment, we experimented in the harsh tabletop environment, which requires higher accuracy and update rate than the room-scale environment, to assess the performance bound of the proposed method. Experimental results showed that our method can estimate the 3-DoF sensor posture of the sensor node with the maximum error of 1.65 degrees and achieved the 3-DoF position estimation with the maximum error of 9.69 mm in the range of 350mm from the reference node. The update rate achieved by the current hardware was 15.16 Hz and enough to provide real-time motion tracking. The update rate of the motion tracking is determined by the time of wireless communication handled by an off-the-shelf BLE circuit. The time profile analysis revealed that our method can track the sensor node with the maximum speed of 28.92 Hz if the performance of the wireless communication is enhanced. Combining the high-performance wireless communication circuit with our method can double the update rate, which is one of our future work.

With the current calculations described in this article, our system cannot tolerate ferrous metallic materials such as steel like other conventional works. S. LaScalza *et al.* report that characterizing the magnetic field distorted by the ferrous metal is very difficult [52]. However, they also suggest that the accuracy of the DC magnetic field-based method could

be improved by tuning the sampling rate according to the collected information about the magnetic permeability of the obstacle. If we scatter a relatively large number of sensor nodes and combine the information from those sensor nodes, the magnetic permeability of the adjacent object could be estimated. Establishing a method which can tolerate the ferrous metallic material is our primary future work.

REFERENCES

[1] K. Shiomi, K. Sato, M. Sawa, and N. Mizukami, "Experimental results of measuring human fatigue by utilizing uttered voice processing," in *Proc. IEEE Int. Conf. Syst., Man Cybern.*, Oct. 2008, pp. 3338–3342.

[2] K. Kiyokawa, M. Hatanaka, K. Hosoda, M. Okada, H. Shigeta, Y. Ishihara, F. Ooshita, H. Kakugawa, S. Kurihara, and K. Moriyama, "Owens luis—A context-aware multi-modal smart office chair in an ambient environment," in *Proc. IEEE Virtual Reality Workshops (VRW)*, Mar. 2012, pp. 1–4.

[3] D. R. Carney, A. J. C. Cuddy, and A. J. Yap, "Power posing: Brief nonverbal displays affect neuroendocrine levels and risk tolerance," *Psychol. Sci.*, vol. 21, no. 10, pp. 1363–1368, Oct. 2010.

[4] I. E. Sutherland, "A head-mounted three dimensional display," in *Proc. Fall Joint Comput. Conf.*, Dec. 1968, pp. 757–764.

[5] K. Kjærside, K. J. Kortbek, H. Hedegaard, and K. Grønbæk, "Ardresscode: Augmented dressing room with tag-based motion tracking and real-time clothes simulation," in *Proc. Central Eur. Multimedia Virtual Reality Conf.*, 2005, pp. 511–515.

[6] T. G. Zimmerman, J. Lanier, C. Blanchard, S. Bryson, and Y. Harvill, "A hand gesture interface device," *ACM SIGCHI Bull.*, vol. 17, pp. 189–192, May 1986.

[7] P. Bellavista, G. Cardone, A. Corradi, and L. Foschini, "Convergence of MANET and WSN in IoT urban scenarios," *IEEE Sensors J.*, vol. 13, no. 10, pp. 3558–3567, Oct. 2013.

[8] L. Da Xu, W. He, and S. Li, "Internet of Things in industries: A survey," *IEEE Trans. Ind. Informat.*, vol. 10, no. 4, pp. 2233–2243, Nov. 2014.

[9] A. Al-Fuqaha, M. Guizani, M. Mohammadi, M. Aledhari, and M. Ayyash, "Internet of Things: A survey on enabling technologies, protocols, and applications," *IEEE Commun. Surveys Tuts.*, vol. 17, no. 4, pp. 2347–2376, 2015.

[10] K. Lin, M. Chen, J. Deng, M. M. Hassan, and G. Fortino, "Enhanced fingerprinting and trajectory prediction for IoT localization in smart buildings," *IEEE Trans. Autom. Sci. Eng.*, vol. 13, no. 3, pp. 1294–1307, Jul. 2016.

[11] C. Perera, A. Zaslavsky, P. Christen, and D. Georgakopoulos, "Context aware computing for the Internet of Things: A survey," *IEEE Commun. Surveys Tuts.*, vol. 16, no. 1, pp. 414–454, 1st Quart., 2014.

[12] M. Botts, G. Percivall, C. Reed, and J. Davidson, "OGC sensor Web enablement: Overview and high level architecture," in *Proc. Int. Conf. GeoSensor Netw.* Cham, Switzerland: Springer, 2006, pp. 175–190.

[13] B. Kim, N. Tomokuni, K. Ohara, T. Tanikawa, K. Ohba, and S. Hirai, "Ubiquitous localization and mapping for robots with ambient intelligence," in *Proc. IEEE/RSJ Int. Conf. Intell. Robots Syst.*, Oct. 2006, pp. 4809–4814.

[14] J. M. DiMicco, A. Pandolfo, and W. Bender, "Influencing group participation with a shared display," in *Proc. ACM Conf. Comput. Supported Cooperat. Work (CSCW)*, 2004, pp. 614–623.

[15] K. Ara, N. Kanehira, D. O. Olguín, B. N. Waber, T. Kim, A. Mohan, P. Gloor, R. Laubacher, D. Oster, A. Pentland, and K. Yano, "Sensible organizations: Changing our businesses and work styles through sensor data," *J. Inf. Process.*, vol. 16, pp. 1–12, 2008.

[16] T. Bergstrom and K. Karahalios, "Conversation votes: Enabling anonymous cues," in *Proc. Extended Abstr. Hum. Factors Comput. Syst. (CHI)*, 2007, pp. 2279–2284.

[17] T. Bergstrom and K. Karahalios, "Conversation clock: Visualizing audio patterns in co-located groups," in *Proc. 40th Annu. Hawaii Int. Conf. Syst. Sci. (HICSS)*, 2007, p. 78.

[18] A. Madan and A. Pentland, "VibeFones: Socially aware mobile phones," in *Proc. 10th IEEE Int. Symp. Wearable Comput.*, Oct. 2006, pp. 109–112.

[19] T. Kim, A. Chang, L. Holland, and A. S. Pentland, "Meeting mediator: Enhancing group collaborationusing sociometric feedback," in *Proc. ACM Conf. Comput. Supported Cooperat. Work (CSCW)*, 2008, pp. 457–466.

[20] K. Fujita, F. Kishino, Y. Itoh, H. Ohsaki, N. Ono, K. Kagawa, K. Takashima, S. Tsugawa, K. Nakajima, and Y. Hayashi, "Ambient suite: Enhancing communication among multiple participants," in *Proc. 8th Int. Conf. Adv. Comput. Entertainment Technol. (ACE)*, 2011, pp. 1–8.

[21] K. Fujita, Y. Itoh, K. Takashima, K. Nakajima, Y. Hayashi, and F. Kishino, "Ambient party room: A room-shaped system enhancing communication for parties or gatherings," in *Proc. IEEE Virtual Reality (VR)*, Mar. 2013, pp. 1–4.

[22] H. Müller, J. Fortmann, M. Pielot, T. Hesselmann, B. Poppinga, W. Heuten, N. Henze, and S. Boll, "Ambix: Designing ambient light information displays," in *Proc. Designing Interact. Lighting Workshop (DIS)*, vol. 10, no. 2317956.2318081, 2012. [Online]. Available: https://dis.acm.org/2020/workshops.html

[23] T. Ozyagcilar, "Implementing a tilt-compensated ecompass using accelerometer and magnetometer sensors," Freescale Semicond., Austin, TX, USA, Tech. Rep. AN4248, 2012, vol. 4248.

[24] H.-J. Chu, G.-J. Tsai, K.-W. Chiang, and T.-T. Duong, "GPS/MEMS INS data fusion and map matching in urban areas," *Sensors*, vol. 13, no. 9, pp. 11280–11288, Aug. 2013.

[25] H. Liu, H. Darabi, P. Banerjee, and J. Liu, "Survey of wireless indoor positioning techniques and systems," *IEEE Trans. Syst., Man, Cybern., C, Appl. Rev.*, vol. 37, no. 6, pp. 1067–1080, Nov. 2007.

[26] M. Andries, O. Simonin, and F. Charpillet, "Localization of humans, objects, and robots interacting on load-sensing floors," *IEEE Sensors J.*, vol. 16, no. 4, pp. 1026–1037, Feb. 2016.

[27] R. Figueiredo, A. Dehban, A. Bernardino, J. Santos-Victor, and H. Araujo, "Shape-based attention for identification and localization of cylindrical objects," in *Proc. Joint IEEE Int. Conf. Develop. Learn. Epigenetic Robot. (ICDL-EpiRob)*, Sep. 2017, pp. 98–103.

[28] D. Murray and A. Basu, "Motion tracking with an active camera," *IEEE Trans. Pattern Anal. Mach. Intell.*, vol. 16, no. 5, pp. 449–459, May 1994.

[29] D. Laurijssen, S. Truijen, W. Saeys, W. Daems, and J. Steckel, "An ultrasonic six degrees-of-freedom pose estimation sensor," *IEEE Sensors J.*, vol. 17, no. 1, pp. 151–159, Jan. 2017.

[30] S. He and S.-H.-G. Chan, "Wi-Fi fingerprint-based indoor positioning: Recent advances and comparisons," *IEEE Commun. Surveys Tuts.*, vol. 18, no. 1, pp. 466–490, 1st Quart., 2016.

[31] C. Yang and H.-R. Shao, "WiFi-based indoor positioning," *IEEE Commun. Mag.*, vol. 53, no. 3, pp. 150–157, Mar. 2015.

[32] C. Wu, Z. Yang, Y. Liu, and W. Xi, "WILL: Wireless indoor localization without site survey," *IEEE Trans. Parallel Distrib. Syst.*, vol. 24, no. 4, pp. 839–848, Apr. 2013.

[33] V. Pasku, A. De Angelis, G. De Angelis, D. D. Arumugam, M. Dionigi, P. Carbone, A. Moschitta, and D. S. Ricketts, "Magnetic field-based positioning systems," *IEEE Commun. Surveys Tuts.*, vol. 19, no. 3, pp. 2003–2017, 3rd Quart., 2017.

[34] W. Kim, J. Song, and F. C. Park, "Closed-form position and orientation estimation for a three-axis electromagnetic tracking system," *IEEE Trans. Ind. Electron.*, vol. 65, no. 5, pp. 4331–4337, May 2018.

[35] J. Huang, T. Mori, K. Takashima, S. Hashi, and Y. Kitamura, "IM6D: Magnetic tracking system with 6-DOF passive markers for dexterous 3D interaction and motion," *ACM Trans. Graph.*, vol. 34, no. 6, p. 217, 2015.

[36] K.-Y. Chen, S. N. Patel, and S. Keller, "Finexus: Tracking precise motions of multiple fingertips using magnetic sensing," in *Proc. CHI Conf. Hum. Factors Comput. Syst.*, May 2016, pp. 1504–1514.

[37] E. Whitmire, L. Trutoiu, R. Cavin, D. Perek, B. Scally, J. Phillips, and S. Patel, "EyeContact: Scleral coil eye tracking for virtual reality," in *Proc. ACM Int. Symp. Wearable Comput.*, Sep. 2016, pp. 184–191.

[38] S. Song, C. Hu, B. Li, X. Li, and M. Q.-H. Meng, "An electromagnetic localization and orientation method based on rotating magnetic dipole," *IEEE Trans. Magn.*, vol. 49, no. 3, pp. 1274–1277, Mar. 2013.

[39] G. De Angelis, V. Pasku, A. De Angelis, M. Dionigi, M. Mongiardo, A. Moschitta, and P. Carbone, "An indoor AC magnetic positioning system," *IEEE Trans. Instrum. Meas.*, vol. 64, no. 5, pp. 1267–1275, May 2015.

[40] F. S. Parizi, E. Whitmire, and S. Patel, "AuraRing: Precise electromagnetic finger tracking," *Proc. ACM Interact., Mobile, Wearable Ubiquitous Technol.*, vol. 3, no. 4, pp. 1–28, Dec. 2019.

[41] E. Whitmire, F. Salemi Parizi, and S. Patel, "Aura: Inside-out electromagnetic controller tracking," in *Proc. 17th Annu. Int. Conf. Mobile Syst., Appl., Services*, Jun. 2019, pp. 300–312.

[42] J. Blankenbach, A. Norrdine, H. Hellmers, and E. Gasparian, "A novel magnetic indoor positioning system for indoor location services," in *Proc. 8th Int. Symp. Location-Based Services*, 2011, pp. 1–11.

[43] J. Blankenbach, A. Norrdine, and H. Hellmers, "A robust and precise 3D indoor positioning system for harsh environments," in *Proc. Int. Conf. Indoor Positioning Indoor Navigat. (IPIN)*, Nov. 2012, pp. 1–8.
[44] P. H. Chen, R. Shirai, and M. Hashimoto, "Coverage-scalable instant tabletop positioning system with self-localizable anchor nodes," in *Proc. 24th Int. Conf. Intell. User Interfaces, Companion*, Mar. 2019, pp. 57–58.
[45] S. H. Yoon, Y. Zhang, K. Huo, and K. Ramani, "TRing: Instant and customizable interactions with objects using an embedded magnet and a finger-worn device," in *Proc. 29th Annu. Symp. User Interface Softw. Technol.*, Oct. 2016, pp. 169–181.
[46] C. Hu, M. Li, S. Song, W. Yang, R. Zhang, and M. Q.-H. Meng, "A cubic 3-axis magnetic sensor array for wirelessly tracking magnet position and orientation," *IEEE Sensors J.*, vol. 10, no. 5, pp. 903–913, May 2010.
[47] R. Shirai and M. Hashimoto, "DC magnetic field based 3D localization with single anchor coil," *IEEE Sensors J.*, vol. 20, no. 7, pp. 3902–3913, Apr. 2020.
[48] D. Roetenberg, H. Luinge, and P. Slycke, "Xsens MVN: Full 6dof human motion tracking using miniature inertial sensors," Xsens Motion Technol. BV, Enschede, The Netherlands, Tech. Rep., 2009, vol. 1.
[49] D. K. Cheng, *Fundamentals of Engineering Electromagnetics*. New York, NY, USA: Addison-Wesley, 1993.
[50] K. Liu, X. Liu, and X. Li, "Guoguo: Enabling fine-grained indoor localization via smartphone," in *Proc. 11th Annu. Int. Conf. Mobile Syst., Appl., services*, 2013, pp. 235–248.
[51] "LSM9DS1 inemo inertial module: 3D accelerometer, 3D gyroscope, 3D magnetometer," S. Microelectronics, LSM9DS1 Datasheet, Mar. 2015.
[52] S. LaScalza, J. Arico, and R. Hughes, "Effect of metal and sampling rate on accuracy of flock of birds electromagnetic tracking system," *J. Biomechanics*, vol. 36, no. 1, pp. 141–144, Jan. 2003.

RYO SHIRAI (Graduate Student Member, IEEE) received the B.E. and M.E. degrees in information systems engineering from Osaka University, Suita, Japan, in 2016 and 2018, respectively, where he is currently pursuing the Ph.D. degree in information science and technology. He has been a Research Fellow of the Japan Society for the Promotion of Science (JSPS) since 2019. His current research interests include analog circuit design, embedded systems, and sensor systems.

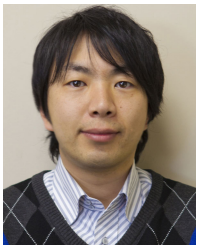

YUICHI ITOH (Member, IEEE) received the B.E. and M.E. degrees in engineering and the Ph.D. degree in information science and technology from Osaka University, Suita, Japan, in 1998, 2000, and 2006, respectively. He is currently an Associate Professor with the Department of Information Systems Engineering, Graduate School of Information Science and Technology, Osaka University. His research interest is to develop novel and intuitive user interfaces for human's daily life.

MASANORI HASHIMOTO (Senior Member, IEEE) received the B.E., M.E., and Ph.D. degrees in communications and computer engineering from Kyoto University, Kyoto, Japan, in 1997, 1999, and 2001, respectively. He is currently a Professor with the Department of Information Systems Engineering, Graduate School of Information Science and Technology, Osaka University, Suita, Japan. His current research interests include the design for manufacturability and reliability, timing and power integrity analysis, reconfigurable computing, soft error characterization, and low-power circuit design. He was a recipient of the Best Paper Award from Asia and South Pacific Design Automation Conference in 2004 and the Best Paper Award of the *IEICE Transactions* in 2016. He was on the Technical Program Committee of international conferences, including the Design Automation Conference, the International Conference on Computer Aided Design, the International Test Conference, the Symposium on VLSI Circuits, ASP-DAC, and DATE. He serves/served as the Editor-in-Chief for *Microelectronics Reliability* (Elsevier) and an Associate Editor for the IEEE TRANSACTIONS ON VERY LARGE SCALE INTEGRATION, IEEE TRANSACTIONS ON CIRCUITS AND SYSTEMS—I: REGULAR PAPERS, and *ACM Transactions on Design Automation of Electronic Systems*.